Sound absorption prediction of linear damped acoustic resonators using a lightweight hybrid model

F. Mbailassem, E. Gourdon, Quentin Leclere, Emmanuel Redon, T. Cambonie

Sound absorption prediction of linear damped acoustic resonators using a lightweight hybrid model

F. Mbailassem[a,b,*], E. Gourdon[a], Q. Leclère[b], E. Redon[c,b], T. Cambonie[a]

[a] *LTDS UMR CNRS 5513, ENTPE, Univ Lyon, F-69518 Vaulx-en-Velin, France*
[b] *Univ. Lyon, INSA-Lyon, LVA EA677, F-69621, Villeurbanne, France*
[c] *Université de Bourgogne, ESIREM, 9 Av. Alain Savary, BP 47 870, 21078 Dijon, France*

Abstract

A lightweight numerical method is developed to predict the sound absorption coefficient of resonators whose cross-section dimensions are significantly larger compared to the viscous and thermal boundary layer's thicknesses. This method is based on the boundary layer theory and on the perturbations theory. According to the perturbations theory, in acoustical domains with large dimensions, the fluid viscosity and thermal conductivity only affect the boundary layers. The model proposed in this article combines the lossless Helmholtz wave equation derived from a perfect fluid hypothesis, with viscosity and thermal conductivity values of a real fluid to compute the sound dissipation of geometrical acoustical attenuators (e.g. resonators). It is therefore referred to as a "Hybrid model". This model is computationally very efficient with regard to visco-thermal models such as the FLNS (Full Linearized Navier-Stokes) model. It remains valid and efficient in a wide range of geometries even when reduced models such as the LRF (Low Reduced Frequency) model cannot be applied. The performances of the Hybrid model was tested on several differently shaped acoustical absorbers based on quarter-wave resonators. The Hybrid model results have been compared with experimental data and FLNS simulations and proved to be accurate and very efficient.

*Corresponding author
Email addresses: fulbert.mbailassem@entpe.fr (F. Mbailassem), emmanuel.gourdon@entpe.fr (E. Gourdon)

Keywords: Viscothermal losses, sound absorption, resonance absorbers, acoustic modeling, boundary layer theory, computation efficiency.

1. Introduction

In building acoustics, the sound level and the reverberation time often have to respect some regulatory values in order to avoid some health issues (hearing deficiency or loss, etc.) and speech intelligibility problems. To fulfill this objective, porous materials[1] are often used to absorb the sound energy and to reduce the reverberation in closed spaces. However, porous materials are often limited by their poor absorptive performance at low frequencies and/or their cost. Research has been developed to improve the performance of porous materials especially in the low-frequencies range. For example Yang *et al.*[2, 3] have developed solutions to increase the sound absorption and/or decrease the resonance frequency. Dupont *et al.*[4] showed that porous materials with a special porosity network (dead-end porosity) could have good absorption performance at low frequencies. However, the manufacturing process of such materials seems to be technically difficult as well as more expensive. As a result, well-designed acoustic resonators (Helmholtz resonator, quarter-wave resonator, etc.) can be used as a valid alternative to dissipate the sound energy especially at low frequencies. Resonators can also be used if the sound source to be treated has a narrow frequency bandwidth. In absence of any absorbent material, the dissipation in a resonator originates from viscous forces and thermal conduction. The design of such sound absorbers requires to have a good model able to describe the actual phenomena taking place during the wave propagation in the resonator.

In general, the isentropic Helmholtz wave equation can be used to describe reasonably well most acoustical problems with no mean flow. In this model, the energy losses are neglected assuming the medium inviscid and with no thermal conductivity. When the dimensions of the propagation domain are much smaller, the lossless assumptions no longer hold and using the isentropic model

would be misleading when performing a prediction study. To integrate the energy losses resulting from the acoustic propagation, several models have been developed. Each model has advantages and drawbacks in terms of computational costs and accuracy.

The more complete model is the so-called FLNS (Full Linearized Navier-Stokes) model which takes into account most of the losses phenomena [5, 6]. The main phenomena are the motion of viscous fluid described by Navier-Stokes equation, the thermal conduction and the inertial effects expressed by the continuity equation. Although the FLNS model is very accurate, it can only be analytically solved for simple geometries like tubes or spheres, and numerical methods are often the only way to solve it. As a result, this model unfortunately is computationally very costly. To reduce the computational costs, many reduced models have been developed based on more or less strong simplifications applied to the FLNS equations[7].

Among these reduced models is the SLNS (Sequential Linearized Navier-Stoke) model proposed by Kampinga *et al.* [8, 9] but also by Sambuc *et al.*[10, 11]. This simplified model is closer to the FLNS model but is significantly more efficient. Like the FLNS model, the SLNS model can be be implemented numerically to domains of any shape. Its efficiency in comparison to the FLNS model comes from the fact that the viscous and the thermal losses are calculated separately in a sequential manner using a few hypotheses. Despite a significant efficiency improvement, the SLNS model remains computationally costly compared to other analytical simplified models such as the LRF model. For instance, Kampinga [8] showed in the case of the Hannink's sample that it takes 1926 seconds to solve one frequency with the FLNS while the SLNS model requires only 148 seconds and the LRF model less than one second (0.001 second).

The LRF model is another reduced model developed by Zwikker and Kosten [12] to describe the sound propagation in tubes taking into account the thermal and viscous losses. This model is computationally very efficient and has the advantage to be analytically solved for geometries with simple cross-sections (circular, square, etc.). The LRF solution covers many asymptotic cases [13] including

the Kirchhoff approximation [14] for "wide tubes" and the Rayleigh solution [15] for "narrow tubes". However, since it is based on a plane wave hypothesis, the LRF model is only valid in the frequency range below the cut-off frequency of the tube, and can only be applied to tubes with uniform or very slowly varying cross-sections [9]. These limitations are the main drawbacks of this model, which is widely considered as the most efficient visco-thermal acoustic model.

In the present work, a computationally lightweight method for predicting the sound absorption coefficient of resonant absorbers, like quarter-wave resonators or other resonators with arbitrary geometries and cross-sections, is proposed. This model is based on considerations similar to those used in the boundary layer model of Bossart[16] in which it is assumed that losses only take place in a narrow layer at the tube boundaries. In this paper, the energy dissipation rate approach [17] is adapted to calculate the sound absorption coefficient of acoustic resonators of various shapes using numerical computation of the lossless Helmholtz wave equation. The objective of this Hybrid model is to provide an efficient estimate of the sound absorption coefficient of absorbing resonators of any cross-sectional geometry. In building applications, quarter-wave resonators have thought to be an interesting approach of noise control. However, since the resonance frequency of quarter-wave resonators is inversely related to the resonator length, using straight resonators to absorb low frequencies requires very long resonators and thicker walls than usual. To address this problem, curved resonators [18] or resonators with strongly varying cross-section have been studied. In these cases however, all the hypotheses of the LRF model are no longer respected, and the resonance frequency is no longer proportionally related to the resonator length. Thus, **(i)** strongly curved resonators [18] and resonators with strongly varying cross-section can no longer be referred as classical quarter-wave resonators, and **(ii)** the LRF model is inadequate for taking into account accurately the effects of geometrical irregularities such as pronounced curvature effects on the visco-thermal losses of the resonator. However, it should be underlined that, as shown in literature, for slightly curved resonator and for slow varying cross sections, the LRF model can be used to provide a first rough es-

timate of resonance frequencies. These observations explains both the need of an efficient and accurate alternative model able to handle more complex geometries, as well as the motivation of this study. Throughout this article, the term efficient (or efficiency) is related to the computation cost.

In this paper, we will first introduce the theory of boundary layer losses. In this context and in relation with the assumptions of the perturbations theory for domains with large cross-section dimensions compared to the boundary layers thicknesses, expressions of the viscous and thermal losses are established. Secondly, an estimation of the sound absorption coefficient from the energy dissipation rate will be presented. Finally, the sound absorption coefficient of a few resonators of different geometries, computed with the proposed model will be presented and discussed through a comparison with both experimental and numerical FLNS results.

2. Theory of boundary layer losses

In acoustics, the sound energy dissipation is mainly due to viscous forces and thermal conduction essentially taking place in the viscous and thermal boundary layers. Deriving from these mechanisms, one can distinguish a viscous boundary layer and a thermal boundary layer. The viscous boundary layer (δ_v) depends on the fluid viscosity (μ) while the thermal boundary layer is function of the fluid thermal conductivity (κ). The boundary layers δ_v and δ_t are both frequency dependent as given by:

$$\delta_v = \sqrt{\frac{2\mu}{\rho_0 \omega}} \tag{1}$$

and

$$\delta_t = \sqrt{\frac{2\kappa}{\rho_0 C_p \omega}}. \tag{2}$$

C_p is the fluid heat capacity at constant temperature and ρ its density. ω is the angular frequency related to the frequency f by: $\omega = 2\pi f$. Fig.1 shows the viscous and thermal boundary layers thicknesses in air in the current (audible) frequency range and at $T = 20°\mathrm{C}$.

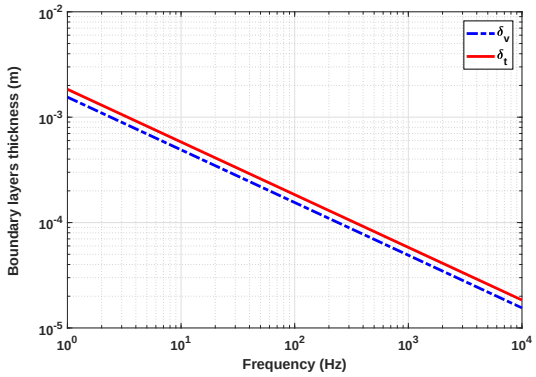

Figure 1: Viscous and thermal boundary layers in air at standard conditions ($1atm$, 20°C)

The losses are due to velocity and temperature gradients between the bulk domain and the boundary surface. The velocity gradient can be explained by the fluid viscosity and the no slip condition at the wall while the thermal gradient happens when this boundary wall is isotherm. In this model the oscillating part of the energy of the propagating sound wave is assumed to be of the form:

$$E(t) = E_0 e^{-\sigma_e t}, \tag{3}$$

and the acoustical pressure can be written by:

$$p(x,t) = p(x) e^{-\sigma_p t} e^{-j\omega t}, \tag{4}$$

where σ_e and σ_p respectively denote for the energy damping rate and pressure damping rate. x is the spatial coordinate, ω, the angular frequency and t is the time in second. σ_e and σ_p are positive quantities expressed in s^{-1} and are related as following [19]:

$$\sigma_e = 2\sigma_p. \tag{5}$$

The damping rate of energy is defined as the ratio of the energy dissipation rate to the total acoustic energy in the system domain[17].

2.1. Viscous losses at a rigid boundary

The viscous laminar boundary losses have been adressed for the first time by Stokes [20] followed then by Kirchhoff [14] and Rayleigh [15]. Since then,

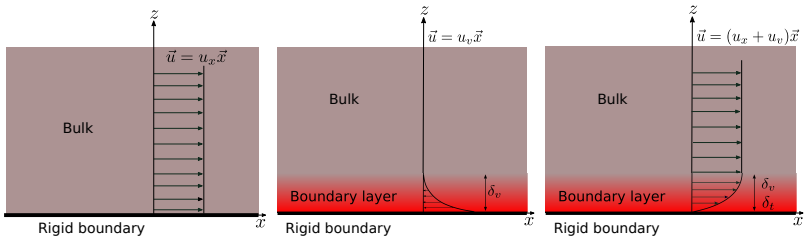

(a) (b) (c)

Figure 2: Acoustic velocity profile of a plane wave. (a) velocity profile in an inviscid fluid, (b) contribution of the fluid viscosity on the acoustic velocity, (c) total velocity in a viscous fluid

many similar developments have been introduced and discussed among which the one presented by Beatty [21] based on Morse theory [22]. In this paper, we use the approach developed by Batchelor [23] in his work on fluids dynamics and presented by Lambert [24] to express the viscous losses taking place at a rigid boundary of a medium in which an acoustical wave propagates.

Let's consider a rigid plane wall bounding a semi-infinite fluid (air for instance). The wall is located in the $z = 0$ plane. If a plane acoustic wave propagates in this fluid in x-direction, the acoustic velocity profile will look like the one presented in Fig.2c where one can easily distinguish two regions: the bulk region with no velocity gradient in the z-direction and the viscous boundary layer (δ_v) shown in red where the velocity increases from zero at the wall boundary to the bulk velocity value at the interface. The total particle velocity $u(x, z)$ (shown in Fig. 2c) of this acoustic wave can be decomposed as a sum of two components:

$$\vec{u} = u\vec{x} = (u_x + u_v)\vec{x} \tag{6}$$

- u_x (shown in Fig. 2a) is constant with regard to the z-coordinate. It corresponds to the acoustic velocity of a wave propagating in a lossless (inviscid) medium.

- u_v (shown in Fig. 2b) is only due to the fluid viscosity[25], and can be seen as the correction made on the total velocity to satisfy the no slip boundary

condition at the wall surface. Therefore $u_v = -u_x$ at the wall surface and vanishes far from the wall surface.

Considering harmonic oscillations, it can be shown [24, 25] that, the viscous part of the particle velocity satisfying the no-slip boundary condition is:

$$u_v = -u_x e^{-(1+j)z/\delta_v} \tag{7}$$

For a bulk velocity of the form $u_x = U_0 e^{(j\omega t - kx)}$, the total velocity u is given by:

$$u = \Re\{U_0[1 - e^{-(1+j)z/\delta_v}]e^{j(\omega t - kx)}\} \tag{8}$$

Moreover, because of the fluid viscosity and the adhesion principle at the boundary, a tangential resistive force is exerted on the surface. The tangential force per unit area is: $F = -\rho\nu(\partial u/\partial z)|_{z=0}$. By taking only the real part into account, it can be shown that[17]:

$$F = \rho\nu\frac{U_x}{\delta_v}[cos(\omega t) - sin(\omega t)], \tag{9}$$

where U_x is the amplitude of the u_x at the boundary given in the general form (even if it can be replaced here by U_0 following the relation $u_x = U_0 e^{(j\omega t - kx)}$). This resistive force leads to an energy loss which can be defined from the instantaneous dissipated energy $dE_s/dt = FU_x$. Averaging this quantity over a time period yields the lost energy per unit area at the boundary due to viscous effects:

$$\left\langle \frac{dE_s}{dt} \right\rangle_v = \frac{1}{2}\rho\nu\frac{U_x^2}{\delta_v} = \frac{1}{2}\rho\nu U_x^2\sqrt{\frac{\omega\nu}{2}} \tag{10}$$

where E_s is the acoustic energy per unit area. The total acoustic power dissipated at the boundary surface by viscous forces can be calculated integrating Eq.10 over the surface of the boundary domain.

$$W_v = \left\langle \frac{dE}{dt} \right\rangle_v = \int_S \left\langle \frac{dE_s}{dt} \right\rangle_v dS \tag{11}$$

To be rigorous, in the real fluid hypothesis in which the "no slip" boundary condition holds, the particle velocity at the boundary layer interface should be

used in Eq.10 instead of U_x. However, for an acoustic domain whose sections have dimensions large enough compared with the boundary layer thickness, the perturbation theory states that in the bulk, the particle velocity is negligibly changed by the viscosity compared to the one in the inviscid fluid. The viscosity influence is significant only in the boundary layer. As a result, the velocity at the boundary layer interface can be approximated by U_x and calculated at the boundary surface using Helmholtz equation in harmonic regime (Eq.12) combined with the Euler equation (Eq.13)

$$\Delta p + k^2 p = 0 \tag{12}$$

$$u = \frac{1}{\rho c_0} p, \tag{13}$$

where k, ρ, and c_0 respectively stand for the acoustic wavenumber, the air density and the acoustic wave speed in the air. The perturbation theory will be valid in any case where the dimensions of an acoustic propagation domain are large in any direction compared with the boundary layer [24] and for small amplitude acoustic fluctuations. Under these conditions, the acoustic damping of the domains is often moderate.

2.2. Thermal losses at rigid boundary surface

In this paragraph, the acoustic energy lost by the thermal conduction at the boundary wall is determined using an approach similar to the one used for the viscous losses. Thus, calculating the thermal losses of an acoustic wave at a conducting surface, requires to know the acoustic temperature (T) distribution in the propagation domain. The Lambert derivation adopted here is similar to Nielson analysis [26] except that the hybrid model does not assume a constant pressure over the wall surface. The starting point of this development is to use the energy equation given by [27]:

$$\kappa \nabla^2 T - j\omega \rho C_p T + j\omega p (C_p - C_v)/R = 0, \tag{14}$$

with:

$$\begin{cases} C_p : \text{specific heat at constant pressure} \\ C_v : \text{specific heat at constant volume} \\ \gamma = C_p/C_v \\ R : \text{Boltzmann's gas content} \end{cases}$$

Using Boyle's Law, Daniels [28] rewrote Eq.14 as:

$$\nabla^2 T = \beta^2 (T - T_a) \tag{15}$$

where $\beta^2 = j\omega\rho_0 Cp/\kappa$ and $T_a = pT_0(\gamma - 1)/(P_0\gamma)$ is the temperature fluctuation in the case of a purely adiabatic compression. κ is the fluid thermal conductivity, ρ_0 its static density, T_0 and P_0 respectively are the static temperature and pressure.

For a gas in which an acoustic wave propagates and which is bounded with a conducting surface with which it exchanges heat, the spatial distribution of acoustic temperature T, the solution of Eq.15 is different of T_a. Considering the similar case of a semi-infinite space filled with a fluid and bounded with an isothermal boundary wall in the $z = 0$ plane, previous works[24, 29] showed that the solution of this equation is

$$T = T_a(1 - e^{-(1+j)z/\delta_t}). \tag{16}$$

This expression of Eq.16 is similar to the one given in Eq.8 for the particle velocity. From this expression, one can easily notice that the temperature vanishes at the wall boundary (i.e for $z = 0$) and approaches the adiabatic value far from the wall ($(z \gg \delta_t)$). In a domain with large enough dimensions, according to the perturbation theory used in the precedent section for viscous losses, the thermal conductivity of the fluid does not affect the bulk domain significantly. The thermal conductivity only affects the thermal boundary layer. In other words, in the bulk domain, the acoustic temperature is in phase with the acoustic pressure, and the thermodynamic transformations are assumed to be adiabatic. Thus,

the temperature T can be expressed as a function of the acoustic pressure:

$$T = \frac{\gamma - 1}{\gamma} \frac{T_0}{P_0} p. \tag{17}$$

In acoustics, the adiabatic oscillations assumption is fulfilled **(i)** for bounded domains (cavities, resonators,etc.) with large dimensions compared with the thermal boundary δ_t (defined by Eq.2), and **(ii)** if the acoustic wavelength λ is such that: $\lambda > 2\pi D_{th}/c_0$, where $D_{th} = \kappa/(\rho_0 c_0)$ is the thermal diffusivity of the gas. The linear relation (Eq.17) between the acoustic temperature and the acoustic pressure can be used to calculate the thermal losses (due to the irreversible flux of heat from the fluid to the wall) as a function of the amplitude of the pressure oscillations. Thus, the damping rate of the energy loss per unit area due to the thermal flux is [24, 17, 30]:

$$\left\langle \frac{dE_s}{dt} \right\rangle_{th} = \frac{1}{2} \frac{\gamma - 1}{\gamma} \frac{|p|^2}{P_0} \sqrt{\frac{\omega D_{th}}{2}} \tag{18}$$

If, in addition, we consider that air is a perfect gas, the adiabatic relation $P_0 = \rho_0 c^2/\gamma$ which links the sound speed to the mean pressure can be used to rewrite equation Eq.18 in the form:

$$\left\langle \frac{dE_s}{dt} \right\rangle_{th} = \frac{1}{2} (\gamma - 1) \frac{|p|^2}{\rho_0 c^2} \sqrt{\frac{\omega D_{th}}{2}}. \tag{19}$$

The total acoustic power W_{th} lost by thermal effect at the boundary area is obtained by integrating the equation (Eq.19) over the boundary surface area S. Thus:

$$W_{th} = \left\langle \frac{dE}{dt} \right\rangle_{th} = \int_S \left\langle \frac{dE_s}{dt} \right\rangle_{th} dS \tag{20}$$

p in the last equations is the spatial acoustic pressure calculated at the interface between thermal boundary layer and the bulk domain. As previously explained in the viscous losses section, under the perturbations theory, the pressure amplitude at this interface may be approximated by the pressure at the boundary wall calculated with the Helmholtz equation (Eq.12). In fact, according to the perturbations theory, for a domain with larger cross-section dimensions in comparison with thermal boundary layer thickness, the thermal conductivity of the

fluid does not affect the bulk domain significantly. Its effect is only limited to the boundary layer.

2.3. Total energy losses

After establishing the expression of the viscous and thermal losses, one can deduce the total energy losses W_{diss} by a simple addition:

$$W_{diss} = \left\langle \frac{dE}{dt} \right\rangle = W_v + W_{th} \tag{21}$$

where E is the total acoustic energy of the system. This energy corresponds to the volume integral of kinetic and potential energy density and is defined by:

$$E = \frac{1}{T_p} \int_{T_p} \int_{V} \left(\frac{1}{2} \rho_0 |u(\mathbf{x}, t)|^2 + \frac{1}{2} \frac{|p(\mathbf{x}, t)|^2}{\rho_0 c^2} \right) \, dV \, dt. \tag{22}$$

T_p is the wave temporal period, $\mathbf{x}$ the domain coordinate (or position). For an harmonic oscillation, equation (Eq.22) becomes:

$$E = \frac{1}{4} \int_{V} \left(\rho_0 |u|^2 + \frac{|p|^2}{\rho_0 c^2} \right) \, dV. \tag{23}$$

Even if a semi-infinite space has been considered to calculate the viscous and thermal boundary layer losses given in equation (Eq.21), this procedure can also be used to obtain an estimate of the boundary losses in closed domains such as cavities or resonators. The only necessary condition to be satisfied is that the domains must have transverse dimensions larger than the viscous and thermal boundary layers thicknesses. The main advantage of using such model is that it is computationally very efficient (see for instance the computation times shown in table 2) since it uses the acoustical velocity and pressure solved from the lossless Helmholtz equation to predict the acoustical dissipation. As a result, this model is by far faster than the full Navier-Stokes model and uses way less computation resources. Since the acoustic quantities (pressure and velocity) computed from the Helmholtz equation (with the inviscid fluid hypothesis) are combined with the boundary layers effects (viscosity and thermal conductivity) to take into account the thermo-viscous losses, we label this model as an "Hybrid model."

3. Estimation of the sound absorption coefficient of resonators

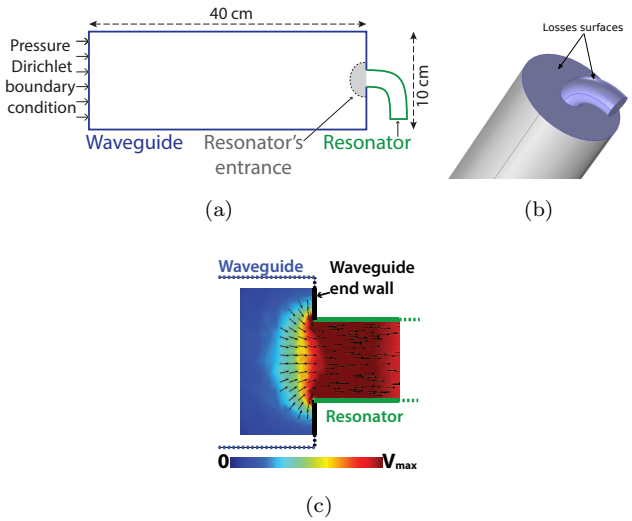

Figure 3: Waveguide used to compute resonator dissipation. (a) resonator connected to a waveguide, (b) losses computation surfaces, (c) Zoomed view over the velocity field at the resonator entrance

The losses quantity W_{diss} given in Eq.21 is homogeneous to a power and therefore corresponds to the dissipated power. If the incident power W_{inc} entering the resonator is known, W_{diss} can be used to compute the acoustical energy dissipated in a resonator and then its sound absorption coefficient α.

The sound absorption coefficient of a given material is defined as the ratio of the power dissipated by this later to the incident power impinging the material ($\alpha = W_{diss}/W_{inc}$). To have the incident power, we chose a geometry where W_{inc} is known and controlled. The dissipative system (in this study various resonators, and for instance a curved tube in Fig. 3) is connected at the end a cylindrical waveguide as shown by Fig.3a. The acoustical pressure and velocity are computed in the whole domain using the lossless Helmholtz wave equation. A pressure (or normal acceleration) Dirichlet boundary condition is applied to the opposite end of the waveguide. To compute the lost power W_{diss}, we consider only the surfaces formed by the resonator and the waveguide top surface

(the blue colored surfaces in Fig.3b) because the losses take place mainly in the resonator. In practice, almost all the losses come from the resonator. But at the resonance frequency, additional viscous losses take place in a small area in the vicinity of the entrance of the resonator which is schematically displayed in grey in Fig.3a. Fig.3c shows a zoomed view of the velocity field in the vicinity of the resonator's entrance. As we can see, even while the wave propagation is perpendicular to the end surface of the bigger tube, the acoustic velocity field streamlines adjust themselves to fit the resonator's entrance, and are therefore no longer perpendicular to the wall. As a result, a certain fraction of the end wall surface can contribute slightly to the overall dissipation (it will be shown further in this paper that this contribution is small). The relevant area of this surface is illustrated in Fig.3a as the interface between the end of the bigger tube and the grey surface. Since it is somehow difficult to determine precisely how far extends around the resonator's entrance the relevant area where the viscous and thermal losses are significant, it can be convenient to use the total end wall area of the bigger tube.

The acoustical pressure in the waveguide is supposed to be quasi-stationnary and can be expressed by:

$$p(x) = A[e^{-jkx} + Re^{jkx}], \tag{24}$$

where again j is the imaginary complex number, A is the incident wave amplitude and R is the sound reflection coefficient. Finally, with the lossless Helmholtz model, one can assume the reflection coefficient to be close to one ($R \approx 1$) and that the above expression can be reduced to:

$$p(x) = 2A\cos(kx). \tag{25}$$

The incident power is given by:

$$W_{inc} = I_{inc} \cdot S = \frac{|A|^2}{2\rho_0 c_0} S \tag{26}$$

where I_{inc} is the incident sound intensity and S the waveguide cross sectional area. From Eq.25, the incident power can be expressed as a function of the

acoustical pressure by:

$$W_{inc} = \frac{|p(x)|^2}{8\rho_0 c_0 \cos^2(kx)} S. \tag{27}$$

Because the expression of Eq.27 is function of x, the incident power is in practice obtained by averaging it along the waveguide length L. After this last operation, one can easily estimate the sound absorption coefficient of the resonator using the relation

$$\alpha = \frac{W_{diss}}{W_{inc}}. \tag{28}$$

This model is valid for damping systems having larger cross-section dimensions (with moderate dissipation in general) in which the the fluid viscosity and thermal conductivity effects are mainly limited at the boundary of the domain. Even if it is so far difficult to quantify the validity limit of this hybrid model in terms of dissipation (sound absorption coefficient for instance), it works when the cross-dimensions are large enough in comparison with boundary layers. For instance, this model would be inadequate for porous materials, where the pores are small and can be roughly the same size than the boundary layers thicknesses. In acoustics, such materials are often modeled with the poroacoustics models in which equivalent fluid properties are determined to take into account viscous and thermal losses, while in the hybrid model developed in this paper, the viscous and thermal losses in rigid boundary cavities are estimated using only the lossless Helmholtz equation.

In addition, since the acoustic wave propagation depends on the temperature of the medium through its effect on the wave celerity, the sound energy dissipation also depends on the quiescent temperature of the propagation medium. Fig.4 shows the effects of the ambient temperature on the sound absorption coefficient of a straight conical quarter-wave resonator computed using the hybrid model. Fig.4 shows that an increase in the temperature significantly shifts the resonance frequency towards higher frequencies (a $\approx$ 50 Hz frequency shift between 20 and 35°C) and slightly increases the absorption level. Therefore, to make possible a relevant comparison with experiments or other analytical

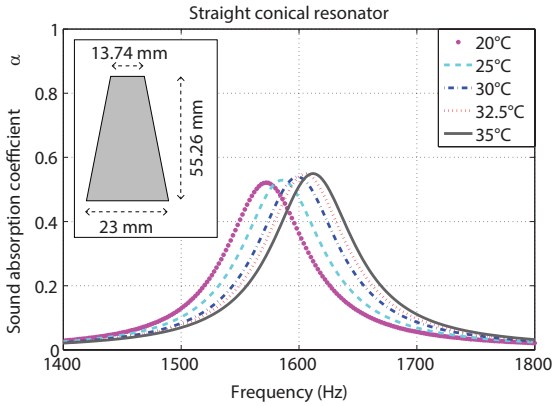

Figure 4: Absolute temperature effects on the sound absorption. All the curves are those of the hybrid model. The conical resonator's dimensions are indicated in the sub-sketch.

or numerical simulations, the temperature dependent parameters used in the hybrid model (as well as in every other numerical model anyway) have to be carefully adjusted to respect the ones of these other studies. This seemingly obvious observation is nevertheless often neglected in the literature while the temperature conditions are often not specified.

4. Validation of the model

In this section, the sound absorption coefficient of resonant absorbers with very varied geometries is predicted with the hybrid model. The geometries investigated satisfy the validity hypotheses of the hybrid model because their cross-sections are all considerably larger than the viscous and thermal boundary layers. The results of these computations are first exposed and then compared with those of the FLNS model and experiments in order to access the model performances and limits.

4.1. Resonators geometry

The investigated geometries are similar to the one (Fig.3) presented in the previous section: various resonators are connected to a waveguide of circular cross-section and are excited with a Dirichlet pressure condition at the opposite

end. The radius of this waveguide is 5 cm while its length is 40 cm (Fig.3a). Five single resonators of different forms and a three resonators system (Fig.5) are used for the validation of the model. The diversity of the investigated geometries illustrates well the range of application of the Hybrid model. Except the straight resonator (Fig. 5a) which has a cross-section of 1 cm radius, all the resonators have 1.15 cm radius at the resonator's entrance (the connecting surface between the resonator and the waveguide). Most of the resonators have a central curvilinear length of 5.526 cm except for the straight and straight conical resonators (Figs. 5a and 5b) which respectively measure 8.55 cm and 6 cm. The choice of these geometries is motivated by the following considerations:

- The straight resonator (Fig.5a) can be seen as a standard benchmark test and gives a preliminary validation of the model. The straight tube corresponds to the classic quarterwave resonator and is indeed the simplest conceivable geometry, on which reduced models such as LRF are valid and accurate.

- The straight conical resonator (Fig.5b) is considered as a first complexity increase, that some models such as the LRF model are unable to take into account. While keeping the axisymetrical symmetry, the effect of a linearly varying cross-section can then be investigated. As stated before, and as shown in Fig. 11, the conical resonator no longer is a classical quarter-wave resonator. Indeed while the resonator's length is kept the same, a 330 Hz difference is observed between the resonance frequencies of the conical resonator and of the straight resonator.

- The curved resonator (Fig.5c) addresses the complementary problem : it corresponds to the case where the cross-section area is kept constant and where the central curvilinear abscissa is no longer straight but bent. A recent work [18] has shown how curvature effects induce modifications of the absorption properties related to the viscous and thermal dissipations in the resonator and explains why the observed resonance frequency differs from the one predicted by the LRF model and shifts toward higher frequencies. The curved

resonator is therefore another interesting benchmark case, complex enough to assess the validity of our model.

- In the curved conical resonator (Fig.5d), the effects of the two last geometries are combined, an unresolvable case for almost every models with the exception of the most complex ones (FLNS, DNS).
- The curved wavy resonator (Fig.5e) igoes further, and demonstrate the hybrid model potential on an resonator with a very complex geometry.
- Finally, the three-resonators system (Fig.5f) is used to extend the scope of the application of the model to coupled resonators interacting with each other.

It is worth noticing that even if the validation of the hybrid model is demonstrated with a few resonators, the range of application of the hybrid model is not only restricted to usual acoustical resonators. It can be applied to a wide range of irregular cavities as long as the model hypotheses are respected. Section 4.4.2.6 discusses the validity range of the hybrid model.

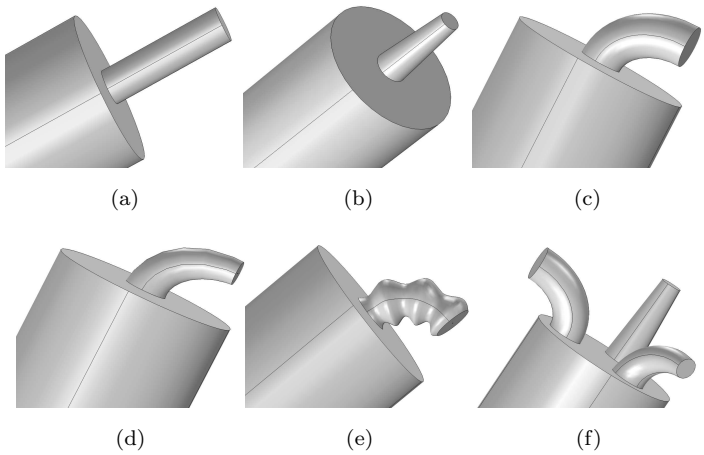

Figure 5: Resonators geometries used for the validation of the hybrid model. (a) straight resonator, (b) straight conical resonator, (c) curved resonator, (d) curved conical resonator, (e) curved wavy resonator, (f) three coupled resonators.

4.2. Numerical procedures

The sound absorption coefficient of the resonator systems presented in the previous subsection is calculated based on pressure and velocity fields numerically computed using Comsol Multiphysics® software. The numerical computations concern both the hybrid model and the FLNS model. For the hybrid model, the pressure and the velocity fields are computed in the coupled system (waveguide-resonator) using the "Frequency study" of Comsol "Pressure Acoustics, Frequency Domain" interface (Helmholtz equation) which can be found in the "Pressure Acoustics" branch under the "Acoustics" module. The domain is meshed with respect to a 10 elements per wavelength criterion based on the maximal frequency. The complete mesh consists of triangular elements created at the top surface of the bigger tube and of two extrusion meshes in the waveguide and in the resonator respectively as shown in Fig.6a.

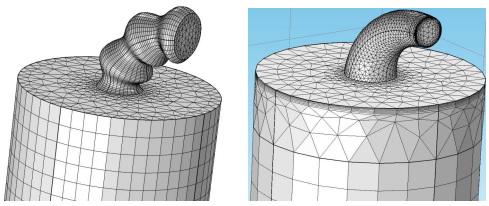

(a) Hybrid model (b) FLNS model

Figure 6: Examples of meshes used in the hybrid model and FLNS model

For the FLNS model, we also computed the acoustical variables (pressure, velocity etc.) using the Comsol "Thermoacoustics, Frequency Domain" interface (FLNS) also available in the "Acoustics" module of the software. The resonator and a small part of the waveguide (in the connection region) are meshed with tetrahedral elements (Fig.6b), the remaining part of the waveguide is meshed by sweeping elements at the interface surface with the already meshed part. In order to compute losses, boundary layers meshing are applied to the resonators boundaries and to the waveguide top surface as indicated in Fig.3b. As we can see on Fig.6, the necessity of adding boundary layers for the FLNS simulation

(Fig.6b) is already one of the reasons explaining why the hybrid model (Fig.6a) is computationally less costly than the FLNS model. In the FLNS model, the acoustic pressures at two 5 *cm* spaced waveguide cross-sections allow to calculate the sound absorption coefficient using the transfer method of ISO $10534-2$ standard [31]. The computation is performed in the frequency domain with a frequency resolution of 1 Hz in a narrow region around the resonance frequency and 2 Hz elsewhere. The FLNS model is applied to all resonators except for the three-resonators system for reasons which will be given later in the results.

4.3. Experimental measurements

In addition to the FLNS model, experiments were conducted to assess the accuracy of the Hybrid model. The resonators of Fig.5 are built with a 3D printer using a rigid and impervious material (Printer: ProJet 3510SD of 3D Systems Europe Ltd., resin: VisiJet M3 Crystal). The resonators samples are presented in the Fig.7. Theses resonators are tested in an impedance tube for measuring their sound absorption coefficient according to ISO $10534-2$ standard. The experimental setup is composed of an acquisition system, a signal amplifier, a signal conditioner and a 100 *mm* diameter **B**&**K** Kundt tube (Fig.8). Following the ISO $10534-2$ method, a 1/4 *in.* microphone is used to measure the acoustical pressure at two 5 *cm* spaced points in the tube in accordance with the standard procedure. The measurement is also made with a frequency resolution 1 Hz. Fig.8 shows the measurement setup used to obtain the experimental sound absorption coefficient of the resonators.
The measurements were carried out in a laboratory at different temperatures. The straight resonator was investigated at 23 °C. For the curved resonator, the wavy resonator and the curved conical resonator, measurements were performed at 31 °C while the two left systems were tested at about 32.5 °C.

4.4. Results and discussion

Fig.10 shows the spectra of the sound absorption coefficient of the various resonators presented in Fig.5 and Fig.7 and compares the hybrid model results

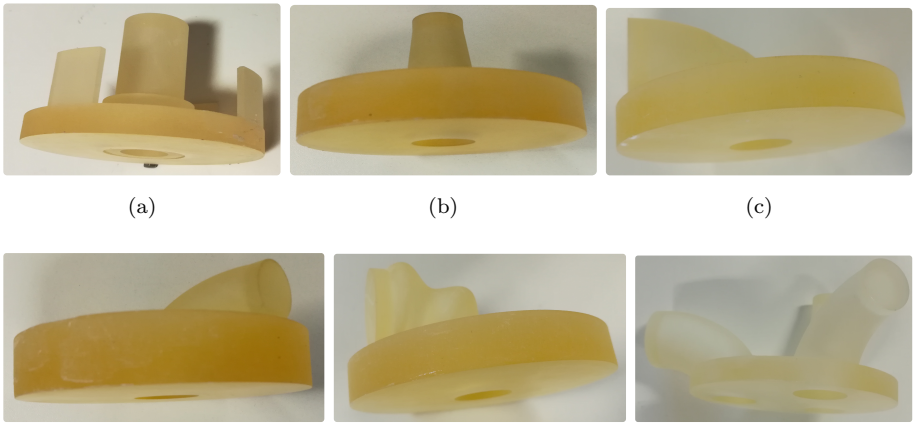

(a) (b) (c)

(d) (e) (f)

Figure 7: Printed resonators. (a) Straight resonator, (b) straight conical resonator, (c) curved resonator, (d) curved conical resonator, (e) curved wavy resonator, and (f) three resonators system.

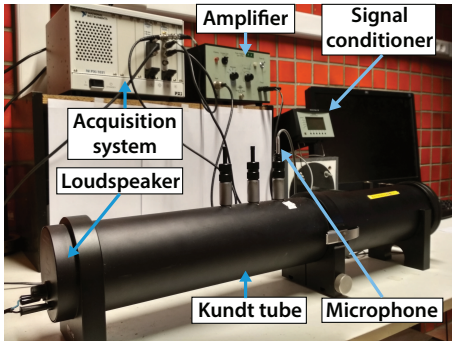

Figure 8: Experimental setup.

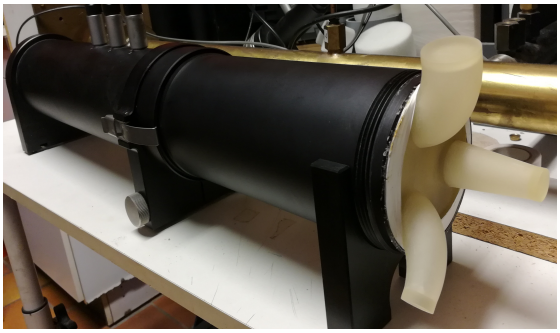

Figure 9: 3-tubes sample in the Kundt tube

with the experimental measurements and other numerical results based on the FLNS model. In order to make a relevant comparison of the efficiency of both models, it is important to specify that both the Hybrid model and the FLNS simulations were computed using a same 32 cores processor work-station (*Intel(R) Xeon Core i7 CPU E5-2665 0 @ 2.4GHz, RAM 64GB*).

The performances of the hybrid model are compared with the FLNS model on one hand and with the experimental results on the other hand. The comparison focuses on :

- on the frequency of the absorption peak in section 4.4.2.1,
- the sound absorption coefficient amplitude in section 4.4.2.2,
- and on the efficiency of the two numerical models in section 4.4.2.5.

The objective is to analyze clearly how accurately and efficiently the hybrid model is able to predict the sound absorption and the resonance frequency of simple geometrical absorbers such as straight resonators, as well as more complex and irregular geometries.

4.4.1. Validation on the straight quarter-wave resonator

For the straight resonator, the sound absorption computed analytically with the LRF model is also plotted for the comparison (Fig.10a).

In most cases, the numerical FLNS is sufficiently accurate to be considered as a reference model [9, 32]. This model was used to validate the LRF model

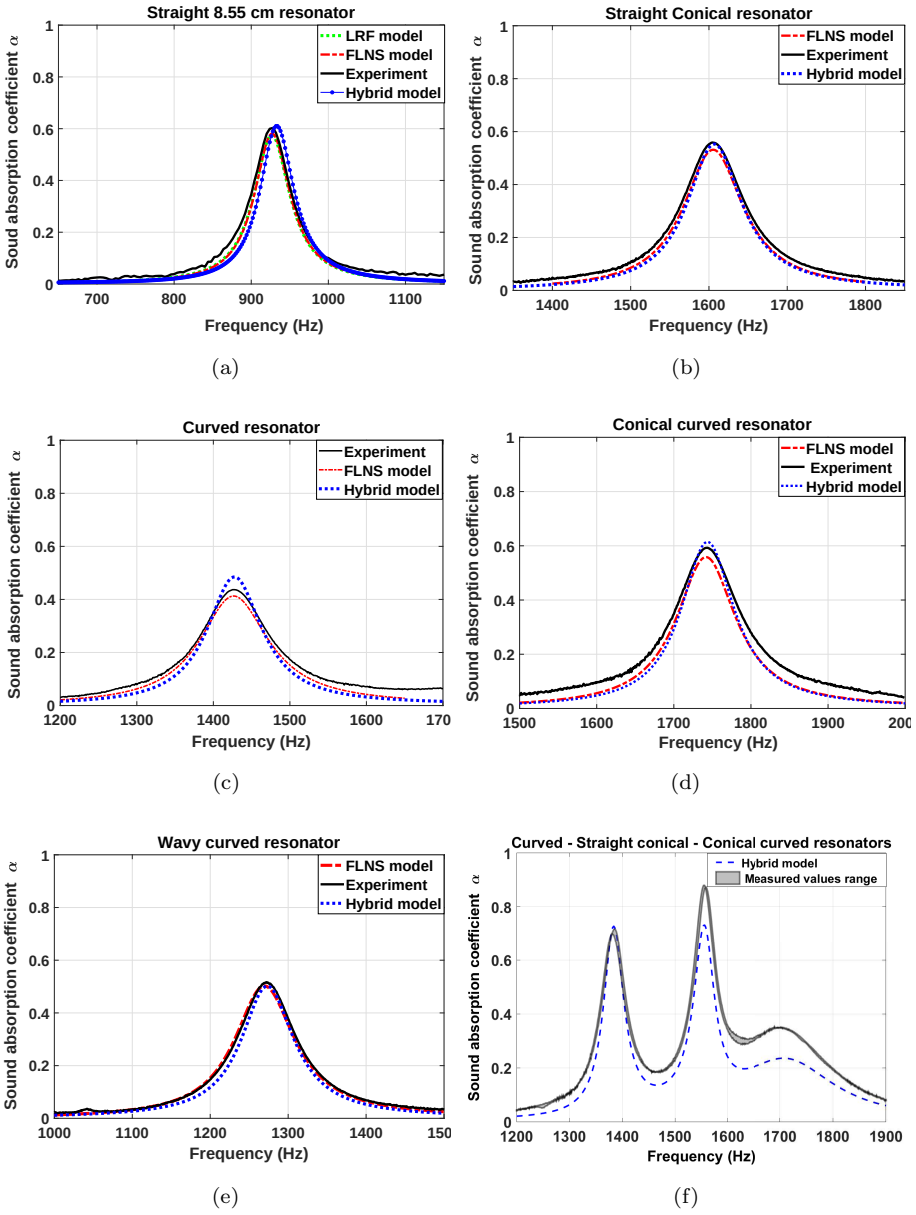

Figure 10: Sound absorption coefficient of the six quarter-wave resonator based absorbers presented above (Cf. Fig.5 and Fig.7)

in the case of the straight resonator as shown in Fig.10a. The FLNS and LRF results closely matches, which confirms the adequacy of the LRF model for tubes with constant cross-section. This validation holds for both the frequency and the sound absorption coefficient amplitude :

- The absorption peak frequencies are $f_{LRF} = 927Hz$ and $f_{FLNS} = 928Hz$.
- The absorption levels (peaks) are $\alpha_{LRF} = 0.575$ and $\alpha_{FLNS} = 0.581$ (i.e. an absorption difference of around 0.006 corresponding to a difference of 1%).

Fig.10a and table 1 both show that on this standard configuration, a straight quarter-wave resonator, the results of the Hybrid model very closely match the predictions of the LRF model and the FLNS simulation.

4.4.2. Validation on more complex geometries

4.4.2.1. Resonance frequency.

We can first underline the accuracy of the Hybrid model predictions concerning the resonance frequency. Indeed the curves of Fig.10 show a very good agreement between the Hybrid model and the FLNS model. The exact values of the frequency of the resonance peak are reported in table 1 to make easier future replication studies or comparisons with other models. The differences do not exceed 4 Hz, a value that is often considered in other numerical studies as negligible, especially in regards with the complexity of the resonator's geometry involved : other very simplified models do not even provide rough estimations (for those specific cases of strongly curved resonators; otherwise LRF model can provide a rough estimate of resonance frequency) of the location of the resonance (especially the LRF model, cf for instance the discussion of Fig. 11 in §4.4.2.2). As we can see this model is able to manage linear (Figs.10b and 10d) and non-linear (Fig. 10e) variations of the cross-section, curvature effects of bended geometries (Figs.10c,10d and 10e), and multiple resonators at the same time (Fig.10f). The comparison with experiments enforces this statement. It shows a very good agreement between the resonance frequencies predicted by

the Hybrid model and the measured one for most of the resonators systems described above. These experiments also validate the numerical results obtained with the FLNS model and proves that the FLNS simulations have been adequately meshed.

It is to be noted is that the resonance frequency of the Hybrid model is always a few hertz higher or equal to that of the FLNS model. This is due to the fact that in a real viscous fluid, the effective sound speed is a little bit smaller than in a perfect fluid [33, 34] as used in the Hybrid model (lossless Helmholtz equation).

	Resonance frequency (Hz)						**Absorption coefficient**					
Single Res.	**Hyb**	**FLNS**	**Meas**	$\mathbf{\Delta f_{HF}}$	$\mathbf{\Delta f_{HM}}$	$\mathbf{\Delta f_{FM}}$	**Hyb**	**FLNS**	**Meas**	$\mathbf{\Delta \alpha_{HF}}$	$\mathbf{\Delta \alpha_{HM}}$	$\mathbf{\Delta \alpha_{FM}}$
straight	932	928	926	4	6	2	0.61	0.581	0.603	0.029	0.007	0.022
curved	1428	1426	1427	2	1	1	0.48	0.415	0.437	0.065	0.043	0.022
straight cone	1606	1606	1605	0	1	1	0.55	0.531	0.559	0.019	0.009	0.028
curved cone	1744	1742	1743	2	1	1	0.61	0.558	0.593	0.052	0.017	0.035
wavy curved	1274	1270	1272	4	2	2	0.505	0.502	0.517	0.003	0.012	0.015
Mean values				2	2.2	1.4				0.0336	0.0176	0.0244
3 tubes	**Hyb**	**FLNS**	**Meas**	$\mathbf{\Delta f_{HF}}$	$\mathbf{\Delta f_{HM}}$	$\mathbf{\Delta f_{FM}}$	**Hyb**	**FLNS**	**Meas**	$\mathbf{\Delta \alpha_{HF}}$	$\mathbf{\Delta \alpha_{HM}}$	$\mathbf{\Delta \alpha_{FM}}$
Peak 1	1384	.	1384	.	0	.	0.728	.	0.708	.	0.020	.
Peak 2	1556	.	1558	.	2	.	0.733	.	0.872	.	0.139	.
Peak 3	1706	.	1702	.	4	.	0.236	.	0.349	.	0.113	.

Table 1: Comparison of the accuracy of the Hybrid model, FLNS model and Experiment. $\mathbf{\Delta f_{HF}}$, $\mathbf{\Delta f_{HM}}$ and $\mathbf{\Delta f_{FM}}$ are respectively the difference between the peak frequencies of the **H**ybrid model and the **M**easurements, the **H**ybrid and the **F**LNS models, and the **F**LNS model and the **M**easurements. Similar notations are adopted for the absorption levels : $\mathbf{\Delta \alpha_{HF}}$, $\mathbf{\Delta \alpha_{HM}}$ and $\mathbf{\Delta \alpha_{FM}}$.

4.4.2.2. Absorption level.

Now, regarding the absorption level, the curves show a quite good agreement between the two models for all single resonators investigated. Table 1 presents the differences of the absorption levels $\mathbf{\Delta \alpha_{HF}}$, $\mathbf{\Delta \alpha_{HM}}$ and $\mathbf{\Delta \alpha_{FM}}$ of the Hybrid model, of the FLNS model and of the measurements. $\mathbf{\Delta \alpha_{HF}}$ and $\mathbf{\Delta \alpha_{HM}}$ respectively compare the absorption level of the Hybrid model, with the ones of the

FLNS model and of the measurements. $\mathbf{\Delta}\alpha_{\mathbf{HF}}$ and $\mathbf{\Delta}\alpha_{\mathbf{HM}}$ never exceed 0.065, a value often considered as acceptable with respect to usual measurement errors according to the authors experience. Mean values $\overline{\mathbf{\Delta}\alpha_{\mathbf{HF}}}$, $\overline{\mathbf{\Delta}\alpha_{\mathbf{HM}}}$ have been computed with respect to the single resonator configuration only (as it will be justified in the following paragraph) and can be considered as useful and relevant indicators to evaluate the performance of the Hybrid model with respect to the results given by the FLNS simulations and the experimental measurements. The mean values respectively are $\overline{\mathbf{\Delta}\alpha_{\mathbf{HF}}} = 0.0336$ and $\overline{\mathbf{\Delta}\alpha_{\mathbf{HM}}} = 0.0176$, thus justifying our previous assertion of a *quite good* agreement between the models and the experiments, especially in regards of the mean difference $\overline{\mathbf{\Delta}\alpha_{\mathbf{FM}}} = 0.0244$ obtained between the FLNS simulations and the experimental measurements. This latest value, $\overline{\mathbf{\Delta}\alpha_{\mathbf{FM}}} = 0.0244$, is a good indicator of the usual discrepancy existing between experiments and simulations.

Only the 3 tubes system shows significant differences between the hybrid model prediction and the measurements: the measured sound absorption is higher than the one given by the model at the second and third resonance frequencies. Our previous studies[1] showed us that such differences of sound absorption level could come from air leaks around the sample and the Kundt tube. Therefore, to be sure of the validity of the experimental measurements, we took care that the 3 tubes system was correctly inserted to avoid air leaks, and the whole experiments have been entirely reproduced five times. The results show a very small deviation of the absorption curves as it is shown in Fig.10f using a grey band encompassing for each frequency the minimal and maximal measured values over all the experiments. Since experimentation errors have been excluded, the most logical hypothesis to explain this difference has to be found in the hypotheses and conditions of the hybrid model. As stated in sections 2.1 and 2.2, under the assumptions of the perturbation theory, for a domain with cross-section dimensions much larger than the viscous and thermal boundary layer

[1] *"Contrôle du bruit par effets de localisation par géométries irrégulières." F. Mbailassem, thesis report, INSA Lyon October 2016.*

thickness, the thermal conductivity and the viscosity of the fluid does not significantly affect the bulk domain, and their effects is focused at the walls in the viscous and thermal boundary layers. But although this assumption which stands for most of the fluid bulk, it does not necessary apply to the small region near the resonator's entrance (Fig.3a) where important visco-thermal effects are observed due to the radiation of the resonator opening in the waveguide. These effects are usually taken into account using a corrected tube length ϵ adjusted from the geometrical characteristics of the resonator and of it surroundings[35]. A potential explanation lies in the proximity of the 3 resonators which makes possible for these region to intersect and interact with each other; an effect that our model is not able to take into account.

The resonance frequency are nevertheless very accurately predicted, and these discrepancies on the absorption level can be considered as marginal compared to the good results given by the hybrid model, as well as a useful reminder of the limitations deriving from the assumptions of this model.
The diversity of the geometries investigated and successfully predicted is in itself a strong result. The Hybrid model can be applied to tubes with large geometrical variations (e.g. wavy resonator) while the LRF can only be applied for straight cylindrical tubes or tubes whose properties varies slowly enough for the geometry to be locally approximated by a cylinder. For instance, when the resonator is strongly bent as shown in [18], the curvature induces effects that are note taken into account at all by the LRF model as it is shown in Fig.11. According to this figure, the sound absorption of a resonator depends on its geometrical form (cross-section and curvature). In the case of the results presented in Fig.11 the LRF model is accurate only for the straight resonator while the resonance frequency of this moderately curved resonator already differs by 20 Hz from the one of the straight resonator. Frequency shifts over 100 Hz (with respect to the straight resonator) have been observed for more strong and abrupt curvatures. For the conical curved resonator and the wavy resonator, the LRF model is accurate neither regarding the frequency nor the absorption level. Nevertheless, compared to the proposed hybrid model, the LRF model

is valid for both narrow and wide tubes while the hybrid model is limited to resonators with large cross-section (cf §4.4.2.6 for a more complete discussion on the Hybrid model limitations). In addition, the LRF model is computationally considerably more efficient than the hybrid model: Kampinga [8] showed an $\approx 2.10^6$ ratio between the computing times of the FLNS and LRF models while only a 30 ratio is found between the FLNS and Hybrid models (cf table 2).

Overall, these results show that the hybrid model predicts the sound absorption of geometrical complex resonators very well. To the authors knowledge, such results on irregular resonators (like the wavy resonator) are few in the literature. The next sub-section gives a quick overview of the state of the art, and focuses on studies showing interesting similarities with our work.

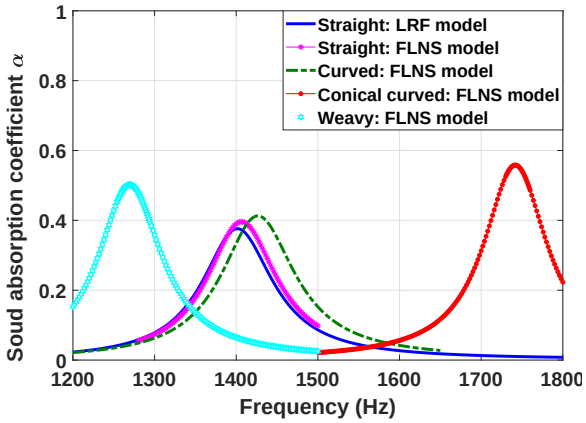

Figure 11: Sound absorption of different quarter-wave based resonators having the same the central curvilinear length of 5.526cm at the same temperature (31.5^{o}C). The curves of this figure show the effect of resonator geometry for a given length.

4.4.2.3. Comparative review with other works.

Cambonie *et al.*[18] recently published a paper about visco-thermal losses in bended quarter-wave resonators, where the curvature effects on the sound absorption properties of resonators are physically explained and predicted, but this works only focused on the case of curved resonators. Moreover, the results of this work have been obtained from numerical FLNS model simulations, after

numerous computationally costly simulations, which could not have been performed on more complex resonator geometries knowing the computing resources at their disposal.

Kampinga [8] and Eerden [33] dealt with prismatic tubes and other irregular resonators to absorb sound energy. To take into account visco-thermal in prismatic tubes, Kampinga used various models from the most complex and complete one (FLNS) to simplified (SLNS) and most simplified one (LRF). The complete models such as the FLNS model are very accurate and can be applied to any geometry but are computationally more costly ($\approx$ 30 computing time ratio, cf table 2) compared to our hybrid model when it can be applied.

Otherwise, Hannink [36] deals with acoustic resonators for the control of noise. However, unlike our study which focuses on the absorption properties, his work focuses on the sound radiation and transmission.

4.4.2.4. A few remarks on the contribution of the bigger tube end.

In this section, we focus on the contribution of the bigger tube end wall to

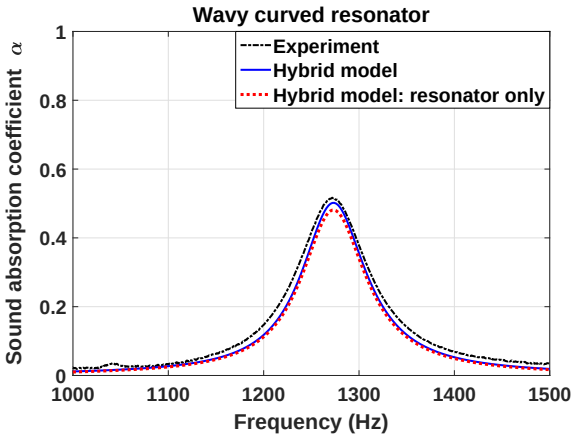

Figure 12: Contribution of the bigger tube end

the overall absorption. As stipulated in section 3, this surface can contribute slightly to the sound absorption, mostly around the resonance frequency of the resonator. In Fig.12 which concerns the wavy resonator, the sound absorption

coefficient of the only resonator surface (without the bigger tube end) obtained with the hybrid model is plotted in addition to the experiment result and the hybrid model result computed with both resonator surface and the bigger tube end surface. According to this figure, the contribution of this surface at the resonance frequency represents only 4.16% of resonator absorption, 4% of the overall absorption and only 3.8% of the experimental absorption peak. In all the investigated cases, the contribution of the bigger tube end represents less than 10% of the total absorption computed with the hybrid model taking into account the resonator and the bigger tube end together.

4.4.2.5. Computational costs and time.

After having investigated the accuracy of the Hybrid model, its efficiency (computational costs) is assessed in this section.

For the three resonators system, the computation configuration (mesh with at least 6 elements per wavelength of the maximal frequency in the waveguide and a boundary layer mesh for the three resonators) was out of memory. This system requires more than the available memory of the powerful computer (64 GB RAM). This incapacity to compute this configuration demonstrates the main limit of the FLNS model in comparison to the hybrid model. It explains why only the results of the hybrid model and the experimental measurements are given in table 1 for the 3 resonators system.

Table 2: Computation time per frequency and used memory

	computation time (s)			**Memory (GB)**	
Resonator	$\mathbf{T_H}$	$\mathbf{T_F}$	$(\mathbf{T_F/T_H})$	**Hyb.**	**FLNS**
curved	34	1025	30	2.39	64
straight cone	29	1134	39	2.2	64
curved cone	31	994	32	2.39	64
wavy curved	23	1208	52	2.3	64

As we can see, the computation time of the FLNS model is **at best 30 times longer** and at worst 52 times longer than the computation time of the Hybrid model as indicated in the table 2. This table not only gives the computation time, but also the physical memory used for the computation of each sample. It

illustrates again the considerably large ratio of computation memory needed for FLNS computations and hybrid ones. Moreover, to emphasize on the efficiency of the proposed hybrid model, it is important to keep in mind that theses results were obtained using the same computer. The Hybrid model is a very efficient (less computationally consuming) model compared to the FLNS model, which is able to accurately predict the sound absorption of numerous irregular and complex geometries such as conical, curved conical and specially curved wavy resonators (Fig.10b, 10d and 10e) using only the lossless and computationally less costly Helmholtz wave equation. From its computational efficiency (costs), the hybrid model is a promising tool for the prediction of sound absorption of systems with irregular and very complex geometries. With the computing resource available for our team, while the FLNS model is unable to compute the system (due to memory constraints of our current system; it is not an inherent limitation of the FLNS model) with only three resonators because of memory deficiency, the hybrid model can be used to predict the sound dissipation of a wall containing a large number of resonators for instance.

4.4.2.6. Limits of validity.

If the boundary layers near two opposite walls overlap, the model is not valid anymore. This condition implies that this model can not be applied to the case of porous materials, micro-perforated structures and other very small cavities. However, this is neither the only nor the most limiting criterion since the boundary layers are very small (around $5.10^{-5}m$ for example at 1000Hz as shown in Figure 1) with respect to the typical size of apertures of classical acoustical resonators. Indeed, for flat and non-flat surfaces, the main limitation of the presented model is the approximation chosen for the calculation of the particle velocity at the boundary layer interface U_x, which is approximately replaced by the velocity calculated at the boundary surface using Helmholtz equation in harmonic regime (Eq.10), under the assumption of a flat velocity profile. It is classically known that different parameters can have an influence on this value: the level of damping, the medium temperature, the velocity amplitude and the

actual velocity profile (linked with the excitation level). All those parameters have an interconnected influence over the effective value of U_x : because they create additional damping, they slightly decrease the effective value of U_x compared to the approximated U_x value obtained using the Helmholtz equation. Therefore, U_x tends to be overestimated, and as a result the lost energy per unit area at the boundary due to viscous effects in Equation (10) is overestimated as well. It leads to a higher predicted sound absorption coefficient than the actual one.

Further studies will focus on understanding how the velocity U_x at the interface of the boundary layer behaves in function of damping, velocity amplitude, surface irregularity,... to extend the validity range of the model.

Although the relevance of these parameters should not be underestimated, the idea behind the hybrid model, which focuses on considering the first order contribution to the viscous and thermal losses, set the main limitations of our model. As outlined in several papers in literature, the validity of models can be expressed in terms of dimensionless parameters which are typically defined by geometric parameters, material parameters (here it does not vary since we consider impervious walls), and frequency. As a result, and similarly to most usual approaches found in the literature to design simplified models, the main design parameters are the characteristic size of the aperture and frequency. That is why only two parameters (frequency and size of aperture) here have been investigated. Nevertheless, as stated in section 2.2, thermal losses are calculated with adiabatic oscillations assumption which is satisfied if the acoustic wavelength λ is such that: $\lambda > 2\pi D_{th}/c_0$, ($D_{th} = \kappa/(\rho_0 c_0)$ is the thermal diffusivity of the gas). In the case of air, this condition is widely fulfilled in frequency range of interest of this study. The size of the aperture has an influence on all the different phenomena responsible for the over-estimation of U_x. For all these reasons, we chose to provide a rough estimated criterion for the model to be valid based on the sizes of the cavities. After many simulations of the hybrid model compared to numerical simulations, it has been found that this typical aperture size must be higher than 1cm to avoid an over estimation of

more than 0.1 on the sound absorption coefficient. For example, in Fig.13 we plot the sound absorption coefficient overestimation at the resonance frequency in function of the radius for a cylindrical resonator of length 10 cm to illustrate the chosen criterion for some simulations.

To illustrate the validity of the frequency range, the difference in the peak absorption amplitude prediction beteween the Hybrid model and the LRF model for different frequencies (different resonator lengths) is plotted in Fig.14. According to this figure, the geomtrical validity presented above is verified.

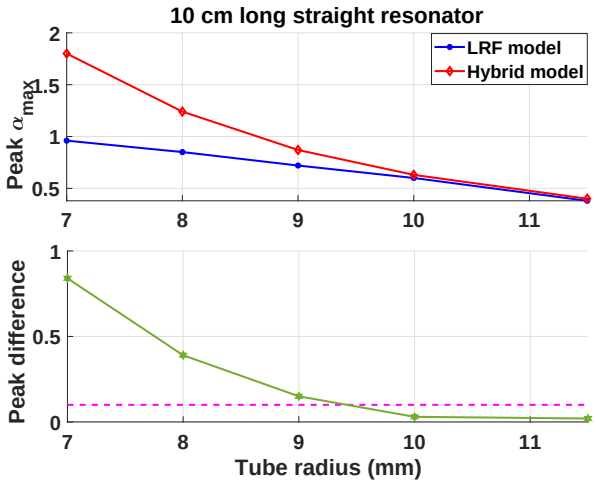

Figure 13: Hybrid model limits shown by a comparison with the LRF model on straight cylindrical tubes of length l0cm. In the top graph, the peaks of sound absorption coefficient obtained with the two models are plotted as function of the tube radius. In the bottom graph the difference between the two models is plotted. The horizontal dashed line represents the threshold gap above which, the validity of the hybrid model no longer holds.

Finally, although all the numerical and experimental test cases shown in this article happen to have circular cross-sections, the underlying hypothesizes used in the hybrid model allow for a wider range of application with more varied cross-section. Of course, smoothly shaped cross-sections (like ellipses) can be dealt with this model, but we also found that non-smooth ones such as rectangular or triangular cross-sections can be successfully carried out. In these cases,

we can obviously expect modifications of the viscous and thermal losses near the corner. Indeed, at the junction between walls the resulting boundary layers are different from having two overlapping boundary layer, but the error made on the estimation of the losses at the corners stays insignificant because the thicknesses of such layers are very small (as stated earlier, $5.10^{-5}m$ at 1000Hz). As a result, as long the as cross-section does not possess too many corners, the relative importance of the corners can be negligible compared with the rest of the cross-section. Under this additional condition, it should also be noted that even if corners introduce an error on the evaluation of the absorption coefficient, this variation is very small and difficult to estimate because other approximations already mentioned have more important effects.

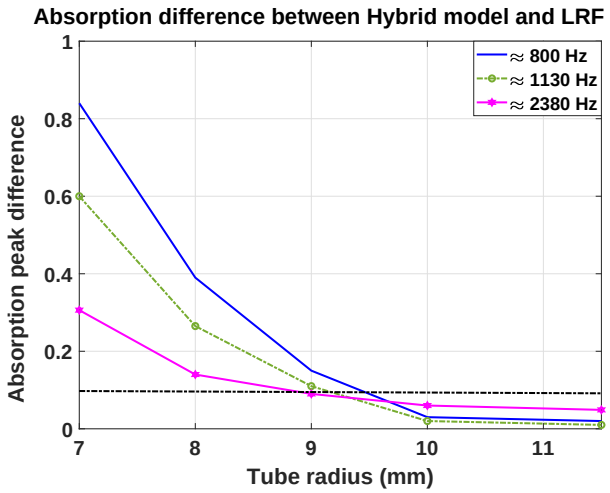

Figure 14: Hybrid model limits shown by a comparison with the LRF model on straight cylindrical tubes for different frequencies (different lengths). The horizontal dashed line represents the threshold gap above which, the validity of the hybrid model no longer holds.

5. Conclusion

A Hybrid lightweight model has been proposed to describe the viscothermal acoustic losses when the air viscosity and thermal conductivity only affect a

narrow region at the boundaries of the considered domain. Thiq model is called "Hybrid" because it is based on the lossless Helmholtz equation while taking into account the fluid viscosity and the fluid thermal conductivity.

This model is adapted to predict the sound absorption coefficient of geometrical acoustic absorbers (such as resonators) of any geometry satisfying this condition.

No less than six resonators of different forms have been investigated to illustrate the potential and the validity range of the Hybrid model. Indeed, each successive geometry has been designed to challenge the predictions of the Hybrid model with increasing levels of complexity. The results have been cross-validated with FLNS simulations and Kundt tube measurements, with which they show very good agreements on both the sound absorption levels and the resonance frequencies. The performances of the Hybrid model are good, since it provides accurate predictions even for very complex geometries such as the curved and wavy resonator.

Moreover, in the present work, a comparison of the computing times of the FLNS and Hybrid models shows a time gain above 30 times with regard to the FLNS.

The Hybrid model can therefore be seen as an efficient and flexible model: like the FLNS model it can be used to investigate resonators with irregular geometries (contrary to the LRF model which is only valid for tubes with constant or very slowly varying cross-sections), and it is furthermore very efficient compared to the FLNS.

For all these reasons, the hybrid model is very promising in building noise control application since its accuracy and efficiency make possible complex computations, involving for instance arrays of complex resonator geometries in parallel.

Further studies will focus on the quantification of the limit of validity of the hybrid model in order to widely benefit from advantages of the model. Also, in addition to push toward a better understanding of its limitations, we would like to modify the Hybrid model to extend its validity range regarding the cross-

section dimensions, as well as the damping level.

Acknowledgements

This work was supported by the Labex CeLyA of Université de Lyon, operated by the French National Research Agency (ANR-10-LABX-0060/ ANR-11-IDEX-0007). This work was also supported by Région Rhône Alpes Auvergne (via european FEDER) in the FUI (21st) project "Actidalle".

References

[1] J. Allard, N. Atalla, Propagation of Sound in Porous Media: Modelling Sound Absorbing Materials 2e, Wiley, 2009.

[2] J. Yang, J. S. Lee, Y. Y. Kim, Metaporous layer to overcome the thickness constraint for broadband sound absorption, Journal of Applied Physics 117 (17) (2015) 174903.

[3] J. Yang, J. S. Lee, Y. Y. Kim, Multiple slow waves in metaporous layers for broadband sound absorption, Journal of Physics D: Applied Physics 50 (1) (2016) 015301.

[4] T. Dupont, P. Leclaire, O. Sicot, X. L. Gong, R. Panneton, Acoustic properties of air-saturated porous materials containing dead-end porosity, Journal of applied physics 110 (9) (2011) 094903.

[5] P. Morse, K. Ingard, Theoretical acoustics, International series in pure and applied physics, McGraw-Hill, 1968.
URL `http://books.google.fr/books?id=EJ0RAQAAIAAJ`

[6] A. Pierce, Acoustics: An Introduction to Its Physical Principles and Applications, Acoustical Society of America, 1989.
URL `http://books.google.fr/books?id=D8GqhULfKfAC`

[7] M. J. J. Nijhof, Viscothermal wave propagation, Ph.D. thesis, Enschede, the Netherlands (December 2010).
URL `http://doc.utwente.nl/74765/`

[8] W. R. Kampinga, Viscothermal acoustics using finite elements : analysis tools for engineers, Ph.D. thesis, Enschede (June 2010).
URL http://doc.utwente.nl/71858/

[9] W. Kampinga, Y. Wijnant, A. de Boer, An efficient finite element model for viscothermal acoustics, Acta Acustica united with Acustica 97 (4) (2011) 618–631.

[10] C. Sambuc, G. Lielens, J. Coyette, Numerical modelling of visco-thermal acoustics using finite elements, 2014.

[11] C. Sambuc, Refined damped equivalent fluid models for acoustics, Ph.D. thesis (2015).

[12] C. Kosten, C. Zwikker, Sound Absorbing Materials, Elsevier, 1949.

[13] H. Tijdeman, On the propagation of sound waves in cylindrical tubes, Journal of Sound and Vibration 39 (1) (1975) 1 – 33. doi:10.1016/S0022-460X(75)80206-9.
URL http://www.sciencedirect.com/science/article/pii/S0022460X75802069

[14] G. Kirchhoff, Ueber den einfluss der wärmeleitung in einem gase auf die schallbewegung, Annalen der Physik 210 (6) (1868) 177–193.

[15] B. J. W. S. Rayleigh, The theory of sound, Vol. 2, Macmillan, 1896.

[16] R. Bossart, N. Joly, M. Bruneau, Hybrid numerical and analytical solutions for acoustic boundary problems in thermo-viscous fluids, Journal of Sound and Vibration 263 (1) (2003) 69 – 84. doi:10.1016/S0022-460X(02)01098-2.
URL http://www.sciencedirect.com/science/article/pii/S0022460X02010982

[17] G. Searby, M. Habiballah, A. Nicole, E. Laroche, Prediction of the efficiency of acoustic damping cavities, Journal of Propulsion and Power 24 (3) (2008) 516–523.

[18] T. Cambonie, F. Mbailassem, E. Gourdon, Bending a quarter wavelength resonator : Curvature effects on sound absorption properties, Applied Acoustics 131 (Supplement C) (2018) 87 – 102. doi:https://doi.org/10.1016/j.apacoust.2017.10.004.
URL http://www.sciencedirect.com/science/article/pii/S0003682X17303146

[19] M. Casiano, T. Zoladz, Theoretical consolidation of acoustic dissipation.

[20] G. G. Stokes, On the communication of vibration from a vibrating body to a surrounding gas, Philosophical Transactions of the Royal Society of London (1868) 447–463.

[21] R. E. Beatty Jr, Boundary layer attenuation of higher order modes in rectangular and circular tubes, The Journal of the Acoustical Society of America 22 (6) (1950) 850–854.

[22] P. M. Morse, Vibration and sound, Vol. 2, McGraw-Hill New York, 1948.

[23] G. K. Batchelor, An introduction to fluid dynamics, Cambridge university press, 2000.

[24] R. F. Lambert, A study of the factors influencing the damping of an acoustical cavity resonator, The Journal of the Acoustical Society of America 25 (6) (1953) 1068–1083.

[25] L. E. Kinsler, A. R. Frey, A. B. Coppens, J. V. Sanders, Fundamentals of acoustics, Fundamentals of Acoustics, 4th Edition, by Lawrence E. Kinsler, Austin R. Frey, Alan B. Coppens, James V. Sanders, pp. 560. ISBN 0-471-84789-5. Wiley-VCH, December 1999. 1.

[26] A. Nielsen, Acoustic Resonators of circular cross-section and with axial symmetry, Transactions of the Danish Academy of Technical Sciences, Akad. for de Tekniske Videnskaber : Gad [in Kommm.], 1949.
URL http://books.google.fr/books?id=aqx3OwAACAAJ

[27] E. C. Wente, The thermophone, Phys. Rev. 19 (1922) 333–345. doi:10.1103/PhysRev.19.333.
URL http://link.aps.org/doi/10.1103/PhysRev.19.333

[28] F. B. Daniels, Acoustical impedance of enclosures, The Journal of the Acoustical Society of America 19 (4) (1947) 569–571. doi:http://dx.doi.org/10.1121/1.1916522.
URL http://scitation.aip.org/content/asa/journal/jasa/19/4/10.1121/1.1916522

[29] S. C. Thompson, J. L. LoPresti, Thermal boundary layer effects on the acoustical impedance of enclosures and consequences for acoustical sensing devices a, The Journal of the Acoustical Society of America 119 (3) (2008) 3377–1370.

[30] T. Shimizu, D. Hori, S. Yoshida, S. Tachibana, S. Matsuyama, J. Shinjo, Y. Mizobuchi, K. Kobayashi, Theoretical and numerical estimation of acoustic damping of a model combustion chamber, AIAA Paper 1146.

[31] ISO, ISO 10534-2 Acoustics, Determination of Sound Abosorption Coefficient and Impedance in Impedance Tubes: Part 2, Transfer-function Method, ISO, 1998.

[32] Y. Wijnant, W. Kampinga, COMSOL's New Thermoacoustics Interface and Computationally Efficient Alternative Formulations for FEM, Comsol, 2011, pp. 1–5.

[33] F. J. M. van der Eerden, Noise reduction with coupled prismatic tubes, Ph.D. thesis, University of Twente, Enschede, the Netherlands (November 2000).
URL http://doc.utwente.nl/32071/

[34] T. Yazaki, Y. Tashiro, T. Biwa, Measurements of sound propagation in narrow tubes, in: Proceedings of the Royal Society of London A: Mathe-

matical, Physical and Engineering Sciences, Vol. 463, The Royal Society, 2007, pp. 2855–2862.

[35] U. Ingard, On the theory and design of acoustic resonators, The Journal of the acoustical society of America 25 (6) (1953) 1037–1061.

[36] M. H. C. Hannink, Acoustic resonators for the reduction of sound radiation and transmission, University of Twente, 2007.